12-17-2012

VEGF and Angiopoietin-1 Exert Opposing Effects on Cell Junctions by Regulating the Rho GEF Syx

Siu P. Ngok
Mayo Clinic Comprehensive Cancer Center, Jacksonville,

Rory Geyer
Mayo Clinic Comprehensive Cancer Center, Jacksonville,

Miaoliang Liu
Dartmouth College

Antonis Kourtidis
Mayo Clinic Comprehensive Cancer Center, Jacksonville,

Sudesh Agrawal
Cleveland Clinic Foundation

See next page for additional authors

Dartmouth Digital Commons Citation

Authors

Siu P. Ngok, Rory Geyer, Miaoliang Liu, Antonis Kourtidis, Sudesh Agrawal, Chuanshen Wu, Himabindu Reddy Seerapu, Laura J. Lewis-Tuffin, Karen L. Moodie, Deborah Huveldt, Ruth Marx, Jay M. Baraban, Peter Storz, Arie Horowitz, and Panos Z. Anastasiadis

VEGF and Angiopoietin-1 exert opposing effects on cell junctions by regulating the Rho GEF Syx

Siu P. Ngok,[1] Rory Geyer,[1] Miaoliang Liu,[2] Antonis Kourtidis,[1] Sudesh Agrawal,[3] Chuanshen Wu,[3] Himabindu Reddy Seerapu,[3] Laura J. Lewis-Tuffin,[1] Karen L. Moodie,[2] Deborah Huveldt,[1] Ruth Marx,[4] Jay M. Baraban,[4] Peter Storz,[1] Arie Horowitz,[3,5] and Panos Z. Anastasiadis[1]

[1]Department of Cancer Biology, Mayo Clinic Comprehensive Cancer Center, Jacksonville, FL 32224
[2]Department of Medicine, Dartmouth Medical School, Lebanon, NH 03756
[3]Department of Molecular Cardiology, Cleveland Clinic Foundation, Cleveland, OH 44195
[4]Solomon H. Snyder Department of Neuroscience, John Hopkins University, Baltimore, MD 21205
[5]Department of Physiology and Biophysics, Case Western Reserve University, Cleveland, OH 44106

Vascular endothelial growth factor (VEGF) and Ang1 (Angiopoietin-1) have opposing effects on vascular permeability, but the molecular basis of these effects is not fully known. We report in this paper that VEGF and Ang1 regulate endothelial cell (EC) junctions by determining the localization of the RhoA-specific guanine nucleotide exchange factor Syx. Syx was recruited to junctions by members of the Crumbs polarity complex and promoted junction integrity by activating Diaphanous. VEGF caused translocation of Syx from cell junctions, promoting junction disassembly, whereas Ang1 maintained Syx at the junctions, inducing junction stabilization. The VEGF-induced translocation of Syx from EC junctions was caused by PKD1 (protein kinase D1)-mediated phosphorylation of Syx at Ser[806], which reduced Syx association to its junctional anchors. In support of the pivotal role of Syx in regulating EC junctions, $syx^{-/-}$ mice had defective junctions, resulting in vascular leakiness, edema, and impaired heart function.

Introduction

Regulation of the paracellular permeability of the endothelial cell (EC) monolayer is essential for the normal function of the vascular system, and its impairment has severe pathological effects. VEGF and Ang1 (Angiopoietin-1) play essential but opposite roles in the regulation of EC junctions and vessel permeability. The molecular mechanisms through which these ligands affect vessel permeability are known partially. VEGF increases vessel permeability by disrupting intercellular junctions through a signaling pathway that includes Src tyrosine kinase (Weis and Cheresh, 2005). Ang1, on the other hand, opposes the effect of VEGF by sequestering Src (Gavard et al., 2008) and stabilizing intercellular junctions. In epithelial cells, junction stability is modulated by the apicobasal polarity complexes CRB (Crumbs–Pals–Patj), PAR (Par3–Par6–atypical PKC), and SCRIB (Scribble–Dlg–Lgl; Tepass, 1996; Qin et al., 2005; Dow and Humbert, 2007). The underlying molecular mechanism and the role of these polarity complexes in EC junction maintenance are unknown.

Rho GTPases constitute a major class of polarity protein and intercellular adhesion effectors (Fukata et al., 2003; Hall, 2005; Iden and Collard, 2008). Junction homeostasis appears to require a precise level of RhoA activity: both hyper- and hypo-activation of RhoA increased paracellular permeability (Braga et al., 1997; Popoff and Geny, 2009; Spindler et al., 2010). Furthermore, the effect of RhoA on cell junctions depends on the agonist: RhoA stabilized junctions in response to Ang1 but destabilized them in response to VEGF (Gavard et al., 2008). The regulation of RhoA by polarity complexes and its signaling at cell junctions are poorly understood.

The Rockefeller University Press $30.00
J. Cell Biol. Vol. 199 No. 7   1103–1115
www.jcb.org/cgi/doi/10.1083/jcb.201207009

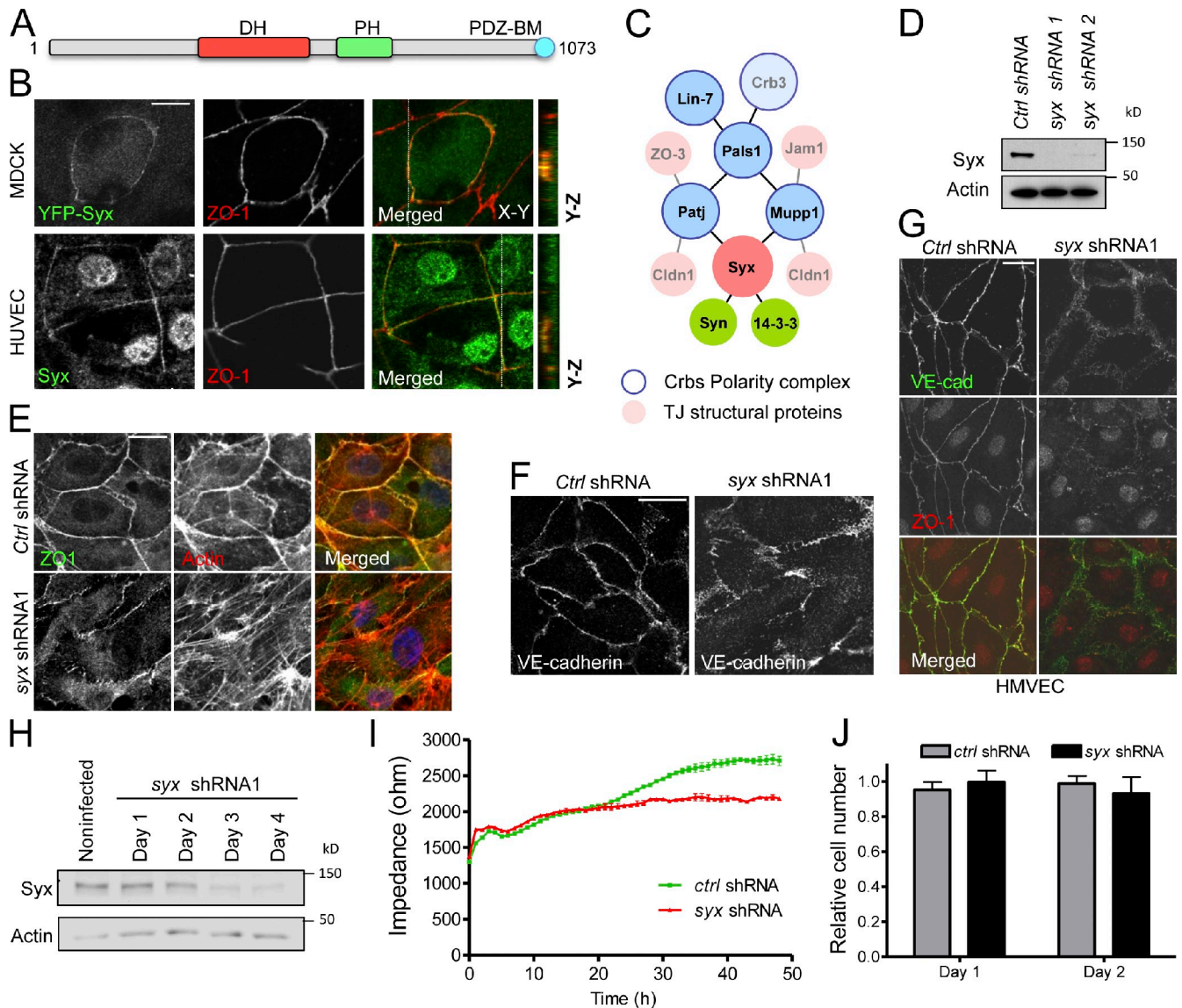JCB   1103

THE JOURNAL OF CELL BIOLOGY

Figure 1. **Syx associates with the CRB polarity complex, localizes at TJs, and is required for maintaining monolayer patency.** (A) Schematic domain structure of Syx. DH, Dbl homology; PH, pleckstrin homology; BM, binding motif. (B) Overexpressed YFP-Syx and endogenous Syx colocalize with the cell junction marker ZO1 in confluent MDCK cells and HUVECs, respectively. The x-z and y-z sections correspond to the white lines. The nuclear staining in HUVECs is likely an artifact, as it is not removed by depletion of endogenous Syx (not depicted). (C) Scheme of the Syx protein complex. The TJ proteins are shown fainter to indicate that their association is inferred from other sources (Syn, synectin; Crbs, Crumbs). (D) Silencing efficacy of the *syx* shRNA constructs in HUVECs. (E) Effect of silencing endogenous Syx on ZO1 and F-actin (phalloidin) localization in HUVECs. (F) Effect of silencing endogenous Syx on the localization of VE-cadherin at the AJs of HUVECs. (G) Effect of silencing endogenous Syx on the localization of VE-cadherin (VE-cad) and ZO1 in HMVECs. (H) Time course of Syx depletion in HUVECs by shRNA1 expression. (I) Effect of silencing endogenous Syx on the impedance of a quiescent HUVEC monolayer. HUVECs infected with either nontarget (*control* [*Ctrl*] shRNA) or *Syx* shRNA1–expressing lentivirus were selected with puromycin for 18–24 h. 48-h postinfection cells were harvested, plated at high confluence (10^5 cells per well), and monitored for their impedance every 180 s for another 48 h (means ± SEM). (J) Quantification of nontargeted (*control* shRNA) versus Syx-depleted (*Syx* shRNA1) HUVEC number. 48-h postinfection cells were harvested and plated at equivalent confluence to cells in I (8×10^5 cells per well in a 6-well plate). The number of live cells was determined by trypan blue exclusion at 1 and 2 d after plating and normalized to the initial plating number. Bars: (B) 10 µm; (E–G) 20 µm.

RhoA binds to and is activated by guanine nucleotide exchange factors (GEFs). We found that the RhoA-specific (De Toledo et al., 2001; Marx et al., 2005) synectin-binding RhoA exchange factor (Syx; Fig. 1 A) is localized to EC tight junctions (TJs). Syx is involved in EC migration (Liu and Horowitz, 2006) and regulates angiogenesis in both the zebrafish and mouse (Garnaas et al., 2008). In this study, we uncovered an unexpected relationship between key members of the CRB polarity complex and the regulation of cell junctions by Syx and RhoA. The localization of Syx, a previously unrecognized member of the CRB polarity complex, emerged as a key factor determining junction stability in vitro and vessel permeability in vivo and conferring the opposite effects of Ang1 and VEGF on EC junctions.

Results

Syx associates with cell junctions and is required for junction integrity

To identify novel regulators of Rho GTPases at cell junctions, we expressed a library of mammalian Rho GEFs in MDCK cells and screened it for junctional localization and for interaction with junctional proteins. Both endogenous and overexpressed YFP-tagged Syx colocalized with ZO1 in human umbilical vein ECs (HUVECs) and in confluent MDCK cells, respectively (Fig. 1 B), indicating that it is a novel junctional Rho GEF.

Using immunoprecipitation of YFP-Syx followed by mass spectrometry analysis, we verified that Syx associated with the scaffold protein Mupp1 (multiple PDZ domain protein 1; Estévez et al., 2008; Ernkvist et al., 2009), synectin (also named Gipc1; Liu and Horowitz, 2006; Ernkvist et al., 2009), Lin7, and the protein associated with Lin7 (Pals1). We also found novel interactions with 14-3-3 proteins; Fig. S1 A and Table S1). These associations, as well as the interaction of Syx with the Mupp1 paralogue Patj (Pals1-associated with TJs), were verified by co-immunoprecipitation and by colocalization of ectopically expressed or endogenous proteins in HUVECs and in neonatal human dermal microvascular ECs (HMVECs; Fig. S1, B–I). With the exception of 14-3-3, the association of these proteins depended on the C-terminal PDZ-binding motif (PBM) of Syx.

Several of the Syx-interacting partners are members of the apical CRB complex (Fig. 1 C), which promotes the integrity of intercellular junctions, as well as apicobasal polarity (Tepass, 1996; Klebes and Knust, 2000; Shin et al., 2005). To determine whether Syx is a key member of this complex, we first tested whether it is required for TJ stability and function. Knockdown of either *syx* or *mupp1* by each of two nonoverlapping shRNAs markedly reduced their expression level (Figs. 1 D and S2 B) and produced a fragmented ZO1 staining pattern in confluent HUVECs and HMVECs (Figs. 1, E and G; and S2, A–C).

The CRB complex has been implicated also in the stability of adherens junctions (AJs), which are required for the maintenance of monolayer integrity (Tepass, 1996; Dejana et al., 2009). Mature AJs reorganize the cortical actin cytoskeleton into circumferential rings that are critical for monolayer integrity. We found that knockdown of *syx* in HUVEC monolayers abolished the circumferential actin localization (Fig. 1 E) and reduced the localization of VE-cadherin to intercellular contact sites in HUVECs (Fig. 1 F) and in HMVECs (Fig. 1 G). The increased distribution of VE-cadherin in the cytosol (Fig. 1 F) correlated with increased VE-cadherin endocytosis in Syx-depleted HUVECs (Fig. S2, D and E).

To determine the functional consequences of the observed junctional defects, we measured trans-endothelial impedance during the formation of postmitotic, confluent HUVEC monolayers expressing *syx* (Fig. 1 H) or control shRNA. The impedance of both monolayers at 4,000 Hz climbed during the first 20 h after plating, but from that point onward, the impedance of the *syx* shRNA-treated monolayer plateaued, indicating that it had achieved its maximum patency. In contrast, the impedance of monolayers treated by control shRNA continued climbing to a plateau higher by ∼30% than the *syx* shRNA-treated monolayers

(Fig. 1 I). The difference in impedance between the two monolayers cannot be attributed to cell density or cell death because cell numbers in each sample were very similar and remained so during the 2 d of the assay (Fig. 1 J). This result indicates that Syx is required for the formation of a fully patent monolayer. Put together, these data indicate that Syx promotes intercellular junction stability and monolayer integrity.

syx$^{-/-}$ mice have defective EC junctions and leaky vessels

We used the angiogenesis-deficient *syx*$^{-/-}$ mouse (Garnaas et al., 2008) to study the in vivo role of Syx in cell junctions. Using ZO1 as a junction marker, we found that it was present as a continuous band in 80% of *syx*$^{+/+}$ ECs but in <20% of *syx*$^{-/-}$ ECs (Fig. 2, A and B), despite a similar expression level (Fig. 2 C). The impedance of *syx*$^{-/-}$ EC monolayers increased at a lower rate than that of *syx*$^{+/+}$ monolayers during the first 4 h and reached a plateau that was lower by 40% than the *syx*$^{+/+}$ impedance at 48 h (Fig. 2 D). Cell numbers in the monolayers of each type were similar (unpublished data). This result indicates that junction formation by *syx*$^{-/-}$ ECs is slower and that their junctions reach a lower steady-state patency compared with *syx*$^{+/+}$ ECs. We then quantified vessel patency in vivo by measuring microsphere extravasation from the tracheal venules of *syx*$^{+/+}$ and *syx*$^{-/-}$ mice. The latter was more than sixfold higher on average than that of *syx*$^{+/+}$ mice (Fig. 2, E and F). Because the vasculature of the *syx*$^{-/-}$ mouse is sparser than that of the *syx*$^{+/+}$ counterpart (Garnaas et al., 2008), the higher extravasation from the *syx*$^{-/-}$ vessels cannot be attributed to a larger vascular length or volume. To rule out the possibility that the leakiness of the *syx*$^{-/-}$ venules reflected defects in non-EC types, we repeated the extravasation assays in a *tie2-Cresyx*$^{fl/fl}$ mouse model. Albeit lower than the extravasation of *syx*$^{-/-}$ venules, the extravasation from *tie2-Cresyx*$^{fl/fl}$ tracheal venules was more than sevenfold higher than in control *syx*$^{fl/fl}$ venules (Fig. 2, E and F). Using transmitted electron microscopy, we observed that the intercellular junctions between mural ECs of *syx*$^{-/-}$ coronary capillaries were malformed or absent (Fig. 2 G). In *syx*$^{+/+}$ mice, areas of intercellular contact between capillary ECs were closely juxtaposed and electron dense. On the other hand, ECs of *syx*$^{-/-}$ capillaries had tenuous intercellular contacts with reduced electron density or did not contact each other at all (Fig. 2 G). Furthermore, erythrocytes were present in the interstitial space of the *Syx*$^{-/-}$ myocardium (Fig. 2 H), consistent with other mouse models exhibiting morphologically similar junctional defects that also suffered from hemorrhage (Cattelino et al., 2003; Feng et al., 2006).

Edema can impair cardiac function by increasing the passive stiffness of the myocardium (Miyamoto et al., 1998; Fischer et al., 2006). To find whether the capillary leakage we observed affected the mechanical properties of the *syx*$^{-/-}$ heart, we measured the pressure–volume relation in *syx*$^{+/+}$ and *syx*$^{-/-}$ left ventricles subjected to partial aortic occlusion. The responses of the *syx*$^{+/+}$ and *syx*$^{-/-}$ left ventricles were vastly different: the difference between the end-diastolic and end-systolic volumes of the *syx*$^{-/-}$ ventricle was much smaller (Fig. 2 I), resulting in a smaller ejection fraction. Because we found no structural differences at the sarcomere level between the *syx*$^{+/+}$ and *syx*$^{-/-}$ myocardia
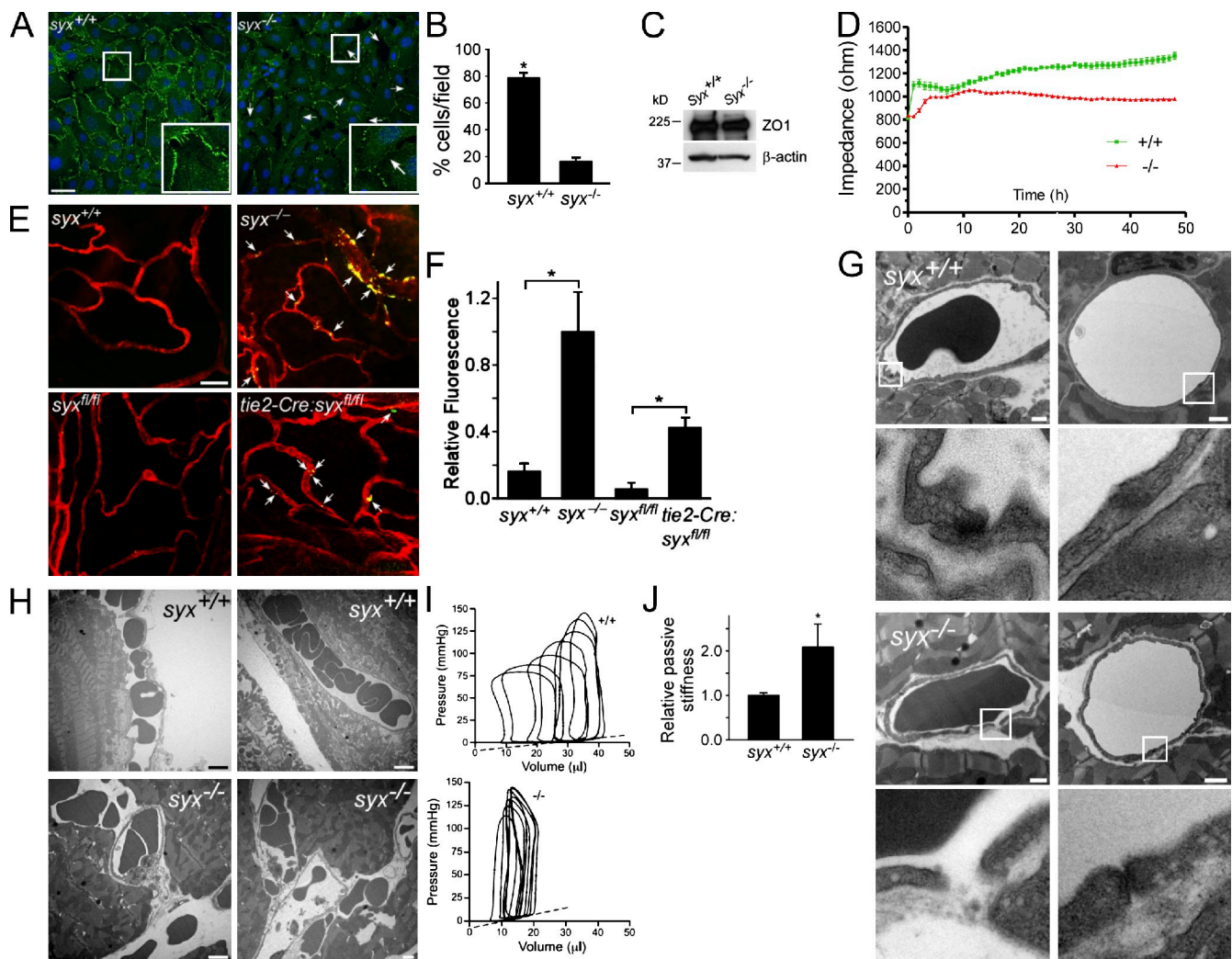
Figure 2. **Cell junction and heart defects in the *syx⁻/⁻* mouse.** (A) Confocal images of confluent monolayers of ZO1-immunolabeled (green) *syx⁺/⁺* and *syx⁻/⁻* ECs, acquired with the same imaging settings. Arrows point to appositions between *syx⁻/⁻* ECs where ZO1 is absent. The framed regions are magnified in the insets. Bar, 50 µm. (B) Quantification of the percentage of ECs surrounded by ZO1 in fields of *syx⁺/⁺* or *syx⁻/⁻* ECs, each containing ∼65 cells (n = 10; ±SEM; *, P < 1.0⁻¹⁰). (C) Expression levels of ZO1 in *syx⁺/⁺* and *syx⁻/⁻* ECs. The β-actin immunoblot is a gel loading control of the ZO1 lanes. (D) *syx⁺/⁺* and *syx⁻/⁻* ECs were plated as confluent monolayers. Impedance at 4,000 Hz was measured every 180 s for 48 h (means ± SEM). (E) Images of *syx⁺/⁺*, *syx⁻/⁻*, *syx^fl/fl*, and *tie2-Cresyx^fl/fl* lectin-stained (red) tracheal venules injected with fluorescent microspheres (green, appearing yellow because of overlap with vessel walls). Arrows point to extravasated microspheres along the walls of *syx⁻/⁻* vessels. Bar, 25 µm. (F) Relative values of extravasated bead fluorescence in images of tracheal vessels (n = 6; ±SEM; *, P < 0.009 and 0.0008). (G) Transmission electron micrographs of thin sections of *syx⁺/⁺* and *syx⁻/⁻* left ventricle myocardium. The junctions between ECs of *syx⁺/⁺* capillaries are sealed, but EC junctions of *syx⁻/⁻* capillaries are open or malformed. The framed regions are magnified below. Bars, 1 µm. (H) Images acquired as in G show that erythrocytes are enclosed within capillaries in the *syx⁺/⁺* myocardium but are present in the interstitial space of the *syx⁻/⁻* myocardium. Bars, 5 µm. (I) Representative series of pressure–volume loops measured in *syx⁺/⁺* and *syx⁻/⁻* left ventricles. Dashed lines denote end-diastolic pressure–volume relation (EDPVR) approximations, whose slopes (0.38 and 0.74 mmHg/µl in the *syx⁺/⁺* and *syx⁻/⁻* ventricles, respectively) represent the passive stiffness of the ventricular wall. The data shown are from a single representative experiment out of three repeats. (J) *syx⁺/⁺* and *syx⁻/⁻* EDPVR slopes (means ± SD; n = 3; *, P = 0.015) normalized by the lowest slope of the *syx⁺/⁺* EDPVR.

(Fig. S2 F), the pressure–volume loop differences are unlikely to result from defective myocardial contractility. The aberrant pressure–volume relation of the *syx⁻/⁻* left ventricle could have been caused, at least in part, by an alteration in the mechanical properties of the walls because of edema. We derived the passive stiffness of the left ventricle by calculating the slope of the linear approximation of the end-diastolic pressure–volume relation (Katz, 2006). The resulting passive stiffness of the *syx⁻/⁻* ventricle was twice as high as that of the *syx⁺/⁺* ventricle (Fig. 2 J). Therefore, our in vitro and in vivo results corroborate each other, showing that Syx is required for the maintenance of EC junctions and blood vessel patency.

Diaphanous (Dia) stabilizes cell junctions downstream of Syx

Previous studies have shown that Syx is a RhoA-specific GEF and that depletion of Syx in ECs results in a significantly reduced RhoA activity (De Toledo et al., 2001; Marx et al., 2005; Liu and Horowitz, 2006). Localized activation of RhoA at epithelial AJs is important for junction assembly and maintenance (Terry et al., 2011). Therefore, we postulated that junction-localized Syx promotes junction stability. To test this premise, we used YFP-Syx, which we previously showed to activate RhoA at the cell membrane (Liu and Horowitz, 2006), and YFP-Syx-ΔPBM (Fig. S3 A), which induces RhoA activation in the cytosol
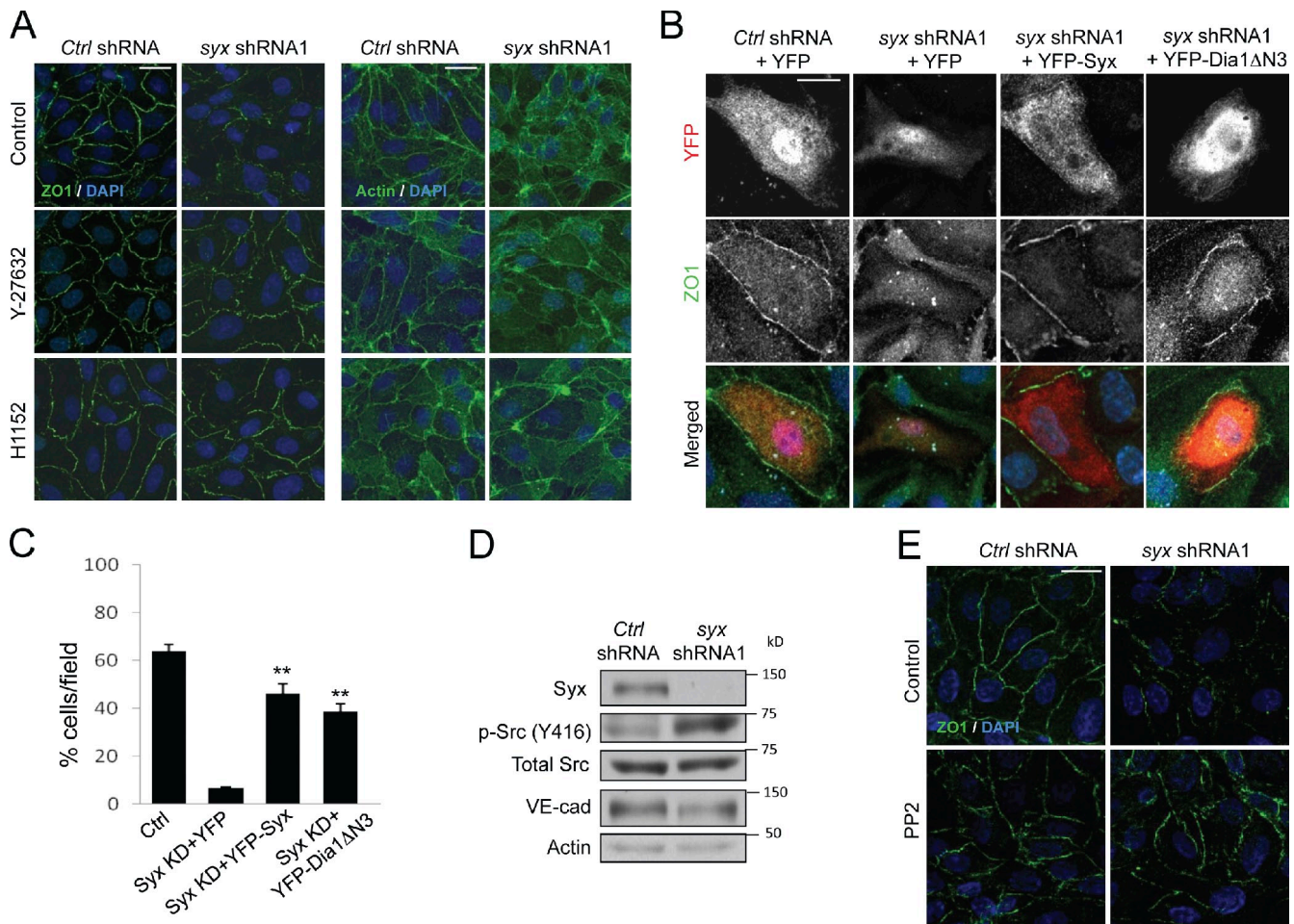
Figure 3.   Dia1 rescues the effects of Syx depletion. (A) Effects of vehicle control, or ROCK inhibition (overnight) with 10 µM Y-27632 or 10 µM H1152 on ZO1 or F-actin (phalloidin) localization in nontarget (*control* [*Ctrl*] shRNA) versus Syx-depleted (*Syx* shRNA1) HUVECs. (B) Effects of transiently expressing YFP alone, YFP-tagged murine Syx (YFP-Syx), or YFP-tagged constitutively active Dia1 (YFP-Dia1ΔN3) on ZO1 pattern in nontarget (*control* shRNA) versus Syx-depleted (Syx shRNA1) HUVECs. (C) Quantification of the percentage of HUVECs from B that express YFP constructs and are surrounded by a continuous and linear ZO1 staining (means ± SEM; ~10 cells per field; n = 6; **, P < 0.001). KD, kinase dead. (D) Effect of silencing Syx on Src phosphorylation at Y416 and total VE-cadherin (VE-cad) levels in HUVECs. (E) Effect of vehicle control or Src inhibition (10 min) with 1 µM PP2 on ZO1 localization in nontarget (*control* shRNA) versus Syx-depleted (*Syx* shRNA1) HUVECs. Bars: (A and E) 20 µm; (B) 10 µm.

(Liu and Horowitz, 2006). Despite inducing equivalent levels of RhoA activation (Fig. S3 B), YFP-Syx localized at intercellular junctions and induced junctional actin accumulation (a telltale sign of mature AJs), whereas YFP-Syx-ΔPBM was cytosolic and increased the number of stress fibers (Fig. S3, C and D). Furthermore, the N terminus region of Syx (Syx-N) inhibited the GEF activity of the endogenous Syx (Fig. S3 E and not depicted) and strongly suppressed junction formation when expressed at low levels, similar to the Rho selective inhibitor C3 exotransferase (Fig. S3 F). These data argue strongly that Syx activates RhoA to promote junction integrity.

The regulation of intercellular junctions and permeability by RhoA is complex and is likely regulated by the subsequent activation of downstream effectors (Braga et al., 1997; Takaishi et al., 1997; Sahai and Marshall, 2002; Wojciak-Stothard and Ridley, 2002; Popoff and Geny, 2009; Terry et al., 2011). Signaling through the RhoA-associated kinases ROCK1 and ROCK2 has been related to both negative (Sahai and Marshall, 2002) and positive (Terry et al., 2011) effects on junction integrity. Suppression of Rho-associated protein kinase (ROCK) activity by

overnight treatment with either Y-27632 or H1152 (10 µM) did not significantly affect junction integrity of control HUVECs, as assessed by ZO1 and actin staining (Fig. 3 A). Instead, ROCK inhibition partially restored junctional ZO1 and actin localization in HUVECs expressing *syx* shRNA (Fig. 3 A). Because ROCK activation cannot account for Syx effects at EC junctions, we next asked whether Dia stabilized junctions downstream of Syx. Dia is thought to prevent VE-cadherin endocytosis and to maintain junctional stability by inhibiting Src (Gavard et al., 2008). Similarly, Dia promotes E-cadherin stabilization and the establishment of a cortical actin ring in epithelial cells (Sahai and Marshall, 2002), downstream of RhoA (Carramusa et al., 2007). We found that expression of a constitutively active N-terminally truncated Dia1 mutant (Dia1ΔN3; Watanabe et al., 1999) in cells depleted of endogenous Syx restored the junctional localization of ZO1 (Fig. 3 B). The Dia-mediated rescue of junctional ZO1 staining was equivalent to that of rescuing Syx-depleted cells by expressing exogenous murine Syx (Fig. 3 C). Consistent with an involvement of Src in these effects, Syx depletion induced the activation of Src kinase (Figs. 3 D and S3 G, quantification),

and pharmacological inhibition of Src in Syx-depleted HUVECs partially restored the junctional localization of ZO1 (Fig. 3 E). Therefore, our data indicate that junction-targeted Syx is required for the localized activation of Dia by RhoA, resulting in the stabilization of intercellular junctions.

Syx acts downstream of CRB polarity members to regulate junction integrity

The interaction of Syx with members of the CRB complex and its localization to cell junctions require the C terminus PBM (Fig. S1, C–E). Synectin and Mupp1 bind directly to Syx via their PDZ domains in yeast two-hybrid screens (Liu and Horowitz, 2006; Estévez et al., 2008; Ernkvist et al., 2009). Furthermore, Pals1 and Mupp1 interact directly via their L27 domains (Roh et al., 2002). Depletion of endogenous Mupp1 reduced the association of Syx with Pals1, without affecting binding of Syx to synectin (Fig. S4 A). In contrast, depletion of Pals1 did not affect the interaction of Syx with Mupp1 but reduced overall Mupp1 levels (Fig. S4 B), in agreement with the effect of Pals1 on the stability of the Mupp1 paralogue Patj (Straight et al., 2006). Similar to Syx, knockdown of Mupp1 also disrupted junction morphology (Figs. 4 A and S2, A–C). However, although depletion of Syx had little effect on the recruitment of Mupp1 to the remaining cell contacts, depletion of Mupp1 abolished the junctional recruitment of either endogenous (Fig. 4 A) or exogenous Syx (Fig. 4 B). The data argue strongly that targeting of Syx to EC junctions requires binding to Mupp1.

Consistent with the hypothesis that Syx acts downstream of the CRB polarity complex to promote junction stabilization, depletion of Mupp1 induced the activation of Src kinase (Fig. 4 C). Similar to Syx-depleted cells (Fig. 3, A and E), inhibition of either ROCK or Src activities largely reversed the junctional defects of Mupp1-depleted cells (Fig. 4 D). Combined, the data argue that Syx is a novel member and a key downstream effector of the CRB polarity complex in the regulation of junction integrity.

Ang1 and VEGF reciprocally regulate the localization of Syx

Endothelial intercellular adhesion is regulated reciprocally by Ang1 and by VEGF. Because cell junction strengthening in response to Ang1 requires Rho-mediated activation of Dia, suppression of Src, and VE-cadherin stabilization (Gavard et al., 2008), we tested whether Ang1-mediated junction stabilization requires Syx. Ang1 treatment increased the localization of Syx at junctions (Fig. 5, A, D, and E, quantitation of Syx intensity at junctions). The junctional accumulation of either VE-cadherin or ZO1 (quantified in Fig. 5 B) was dramatically disrupted in cells expressing *syx*-targeted shRNA and was not rescued by treating cells with Ang1. Consistent with this, Syx depletion prevented the Ang1-induced enhancement of barrier function. The role of Syx in the regulation of barrier function by Ang1 was determined by measuring the impedance of postmitotic, confluent HUVEC monolayers treated by control or by *syx* shRNA. Whereas Ang1 increased the impedance of the control monolayers, it had no effect on the impedance of cells treated by *syx* shRNA (Fig. 5 C).

In contrast to Ang1, VEGF disrupts EC junctions (Olsson et al., 2006). In accordance, VEGF treatment (Fig. S4 C) had the same effect as depletion of Syx (Fig. 1, E and F) on VE-cadherin and ZO1 localization at cell junctions and on cortical actin organization. Strikingly, VEGF caused displacement of Syx from cell junctions at a time when the junctional ZO1 pattern became irregular, suggesting that TJs were disassembling (Figs. 5, D and E, quantification; and S4 G). Importantly, this loss of Syx from cell junctions was blocked by pretreatment for 15 min with Ang1 (Fig. 5, D and E). Ang1 pretreatment also prevented the VEGF-induced loss of junctional integrity, as reflected in the increased accumulation of VE-cadherin and ZO1 at cell junctions. We also compared the relative impedance of quiescent HUVEC monolayers treated with PBS to those treated with VEGF, Ang1, or Ang1 together with VEGF. VEGF caused an early increase followed by a sustained decrease in monolayer impedance (Fig. 5 F). Ang1 induced a small increase in impedance, probably because the monolayer had already reached full patency. Ang1 pretreatment (15 min) delayed and largely negated the VEGF effect during the 60-min observation period, suggesting that barrier function closely correlates with Syx localization.

To test whether Syx regulates EC junctions in vivo, we compared the leakage of Evans blue dye from the skin of $syx^{+/+}$ and $syx^{-/-}$ mice in response to injections of PBS, VEGF-A$_{165}$, or Ang1. The leakage of dye from the $syx^{-/-}$ skin was more than threefold higher than the $syx^{+/+}$ skin (Fig. 5 G). VEGF treatment did not further increase the leakiness of $syx^{-/-}$ skin. Moreover, Ang1 was ineffective in diminishing the leakage from the $syx^{-/-}$ skin, in contrast to the $syx^{+/+}$ skin. The leakage from Ang1-treated $syx^{-/-}$ skin was close to ninefold higher than the leakage from $syx^{+/+}$ skin. Therefore, the in vivo data are consistent with the sustained responses of our ECs in vitro to either VEGF or Ang1. Collectively, the data support a model whereby VEGF induces junction disassembly and increases monolayer permeability by displacing Syx from the junctions, and conversely, Ang1 stabilizes junctions and sustains vessel patency at least in part by maintaining Syx at the junctions.

Phosphorylation downstream of VEGF and PKD1 regulates Syx localization

To determine whether VEGF induces the loss of junctional Syx by promoting its dissociation from Mupp1, we immunoprecipitated endogenous Syx from control (PBS) or from VEGF-treated HUVECs. Fig. 6 A (quantitation of Mupp1 bands in Fig. S4 D) shows that less Mupp1 was coimmunoprecipitated by Syx in VEGF-treated cells. Further supporting the dissociation of Syx from Mupp1, VEGF treatment had little effect on the junctional localization of Mupp1 (Fig. S4, E and F). A clue to the mechanism by which VEGF affects Syx localization came from the observation that PMA induced identical effects to VEGF on Syx localization and on ZO1 pattern in HUVECs (Fig. S4 G). As PKD is a critical downstream effector of both VEGF- and PMA-induced angiogenesis (Fig. S4 H; Taylor et al., 2006; Altschmied and Haendeler, 2008; Ha and Jin, 2009), we asked whether it regulates Syx-Mupp1 binding and alters Syx's subcellular localization. Using an antibody (pMotif) that recognizes PKD-phosphorylated motifs (Döppler et al., 2005), we detected
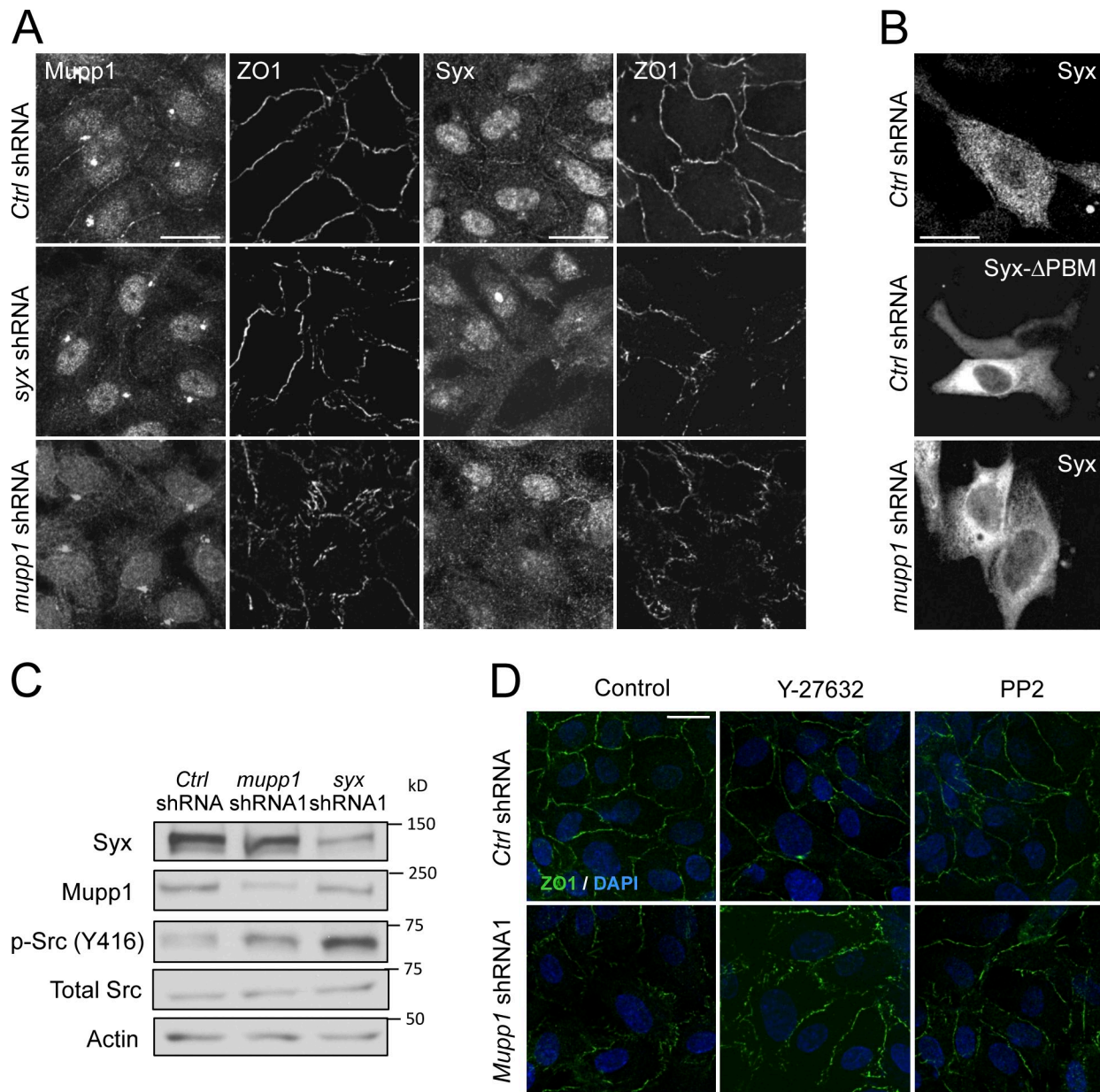
Figure 4. **Syx acts downstream of Mupp1 to regulate junction integrity.** (A) Effect of silencing Syx (*Syx* shRNA) on the localization of endogenous Mupp1 and that of silencing Mupp1 (*Mupp1* shRNA) on the localization of endogenous Syx in confluent HUVECs. ZO1, which colocalizes with Syx and Mupp1 in control HUVECs expressing nontarget shRNA (*control* [*ctrl*] shRNA) is also shown as a measure of cell junction integrity. (B) Effect of expressing a mutant YFP-tagged murine Syx lacking the PBM (Syx-ΔPBM) in control HUVECs expressing nontarget shRNA (*control* shRNA) or of expressing YFP-Syx in cells expressing *Mupp1* shRNA on the targeting of ectopic Syx to the cell periphery. (C) Effect of silencing Mupp1 on Src phosphorylation at Y416 in HUVECs. (D) Effect of vehicle control, inhibition of ROCK (overnight) with 10 μM Y-27632, or inhibition of Src (10 min) with 1 μM PP2 on ZO1 localization in nontarget (*control* shRNA) versus Mupp1-depleted (*Mupp1* shRNA1) HUVECs. Bars, 20 μm.

selective phosphorylation of immunoprecipitated YFP-Syx but not of the other 21 Rho GEFs tested (Fig. S5 A). PMA treatment (Fig. S5 B) and overexpression of either wild-type or constitutively active (but not kinase dead) PKD1 (Fig. S5 C) increased the phosphorylation level of Syx. Importantly, phosphorylation of YFP-Syx was blocked by silencing endogenous *pkd1* and *pkd2* (Fig. S5 D). Consistent with these results and with the high level of PKD1 expression in HUVECs (Fig. S5 E), we observed a significant increase in Syx phosphorylation in VEGF-treated HUVECs (Fig. 6 B). Additionally, PKD1 colocalized with Syx at cell junctions and in the cytoplasm after VEGF treatment

(unpublished data). Finally, as with VEGF, the increase in Syx phosphorylation in response to PMA correlated strongly with decreased binding between Syx and Mupp1 (Fig. S5, F and G).

A potential PKD phosphorylation site was detected in Syx by deletion mutagenesis in the C terminus region beyond residue 757 (Fig. S5 H). Sequence analysis identified two potential PKD phosphorylation motifs in that region, at Ser[806] and Ser[938] (Fig. S5 I), whereas phosphopeptide mapping identified an additional site at Ser[964]. Mutation of Ser[938] and Ser[964] to Ala did not reduce recognition by the pMotif antibody upon PKD overexpression. Recognition was abolished, however, by mutating Ser[806] to Ala
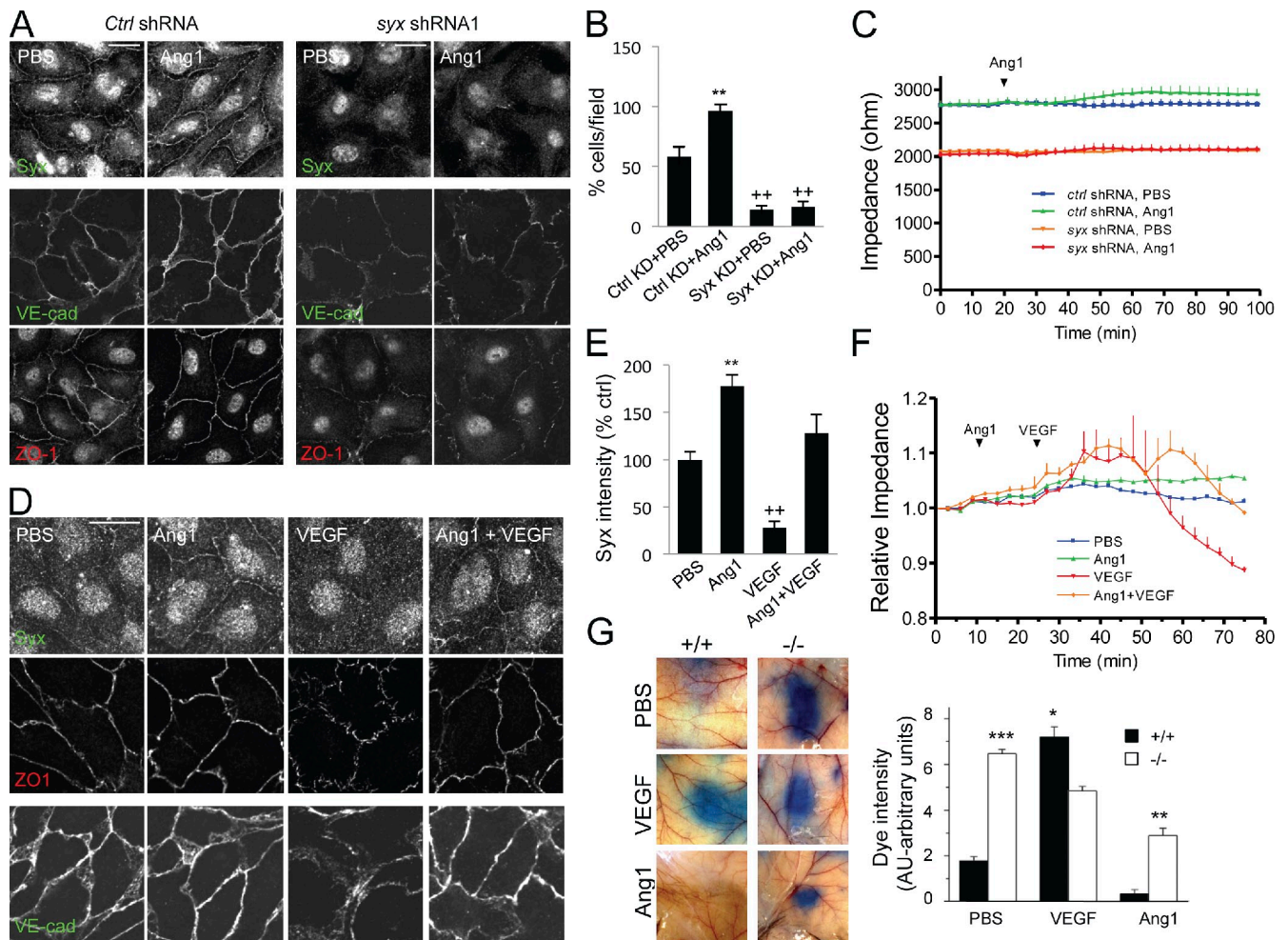
Figure 5. **Ang1 and VEGF have opposing effects on Syx localization.** (A) Effects of Angiopoietin-1 (Ang1) treatment (50 ng/ml for 45 min) on endogenous Syx, VE-cadherin (VE-cad), and ZO1 localization in nontarget (*control* [*Ctrl*] shRNA) versus Syx-depleted (*Syx* shRNA1) HUVECs. The nuclear ZO1 staining is an artifact of the rabbit antibody used here to visualize ZO1. (B) Quantification of the mean intensity of ZO1 at the junctions using ImageJ software (means ± SEM [error bars]; ∼30 cells per field; $n = 6$; **/++, $P < 0.001$, compared with *control* kinase dead + PBS). (C) Effects of Ang1 treatment on the impedance of Syx-depleted HUVEC monolayers. Nontarget (*control* shRNA) versus Syx-depleted (*Syx* shRNA1) HUVECs were grown in ECIS Cultureware Electrode Arrays for 48 h (as in Fig. 1I). Control (PBS) and Ang1 treatments were administered simultaneously as indicated, and impedance was measured every 180 s for the duration of the experiment. Results are representative of three independent experiments performed in triplicate. (means ± SEM). (D) Effects of Ang1 alone (45 min), VEGF alone (30 min), or cotreatment with Ang1 and VEGF (15 min with Ang1 followed by 30 min with VEGF) on Syx, ZO1, and VE-cadherin localization in HUVECs. (E) Quantification of the mean intensity of Syx at the junctions using ImageJ software and expressed as a percentage of control (PBS; means ± SEM; ∼10 cells per field; $n = 6$; **/++, $P < 0.001$, compared with PBS). (F) Effects of Ang1 alone (50 ng/ml), VEGF alone (50 ng/ml), or cotreatment with Ang1 and VEGF (15-min Ang1 pretreatment followed by VEGF, see arrows) on the impedance of quiescent HUVEC monolayers. Impedance values were normalized to the initial values at the beginning of the experiment and are plotted as relative impedance where the baseline value is set at 1.0 (means ± SEM). Results are representative of three independent experiments performed in triplicate. (G) Leakage of Evans blue dye from the skin of $syx^{+/+}$ and $syx^{-/-}$ mice in response to injections of PBS, 10 ng/ml VEGF-A$_{165}$, or 50 ng/ml Ang1 as seen in images of the injections sites. The mean leakage in response to each type of injection is shown in the histogram (means ± SEM; $n = 5$). *, $P < 0.05$; **, $P < 0.01$; ***, $P < 0.001$. Bars, 20 µm.

(Fig. S5 J). The possibility that another kinase acting downstream of PKD phosphorylates Syx at a classical PKD consensus motif cannot be excluded by our data but is unlikely. The simplest explanation is that VEGF and PMA induce Syx phosphorylation at Ser[806] by a common downstream effector, PKD, disrupting Syx binding to Mupp1 and, therefore, Syx localization to cell junctions.

Because Syx phosphorylation correlated with reduced association to Mupp1 (Figs. 6, A and B; and S5, F and G), we asked whether phosphorylation at Ser[806] could regulate the binding of Syx to Mupp1 and thus affect the junctional localization and function of Syx. First, we used YFP as a tag to immunoprecipitate

full-length YFP-Syx or Syx carrying a S806A mutation from HeLa cells overexpressing PKD1. The amount of Mupp1 coimmunoprecipitated with Syx-S806A was approximately twice larger than the one coimmunoprecipitated with Syx (Fig. 6 C), confirming that S[806] regulates Syx binding to Mupp1. When expressed in HUVECs, more cells expressing YFP-Syx-S806A exhibited junctional Syx localization than cells expressing YFP-Syx (Fig. 6, D and E). Importantly, VEGF treatment abolished the junctional localization of YFP-Syx but failed to significantly affect the localization of YFP-Syx-S806A at cell junctions (Fig. 6, D and E). These data indicate that phosphorylation of Syx at S[806] is a major mechanism by which VEGF regulates the recruitment of Syx to EC junctions.
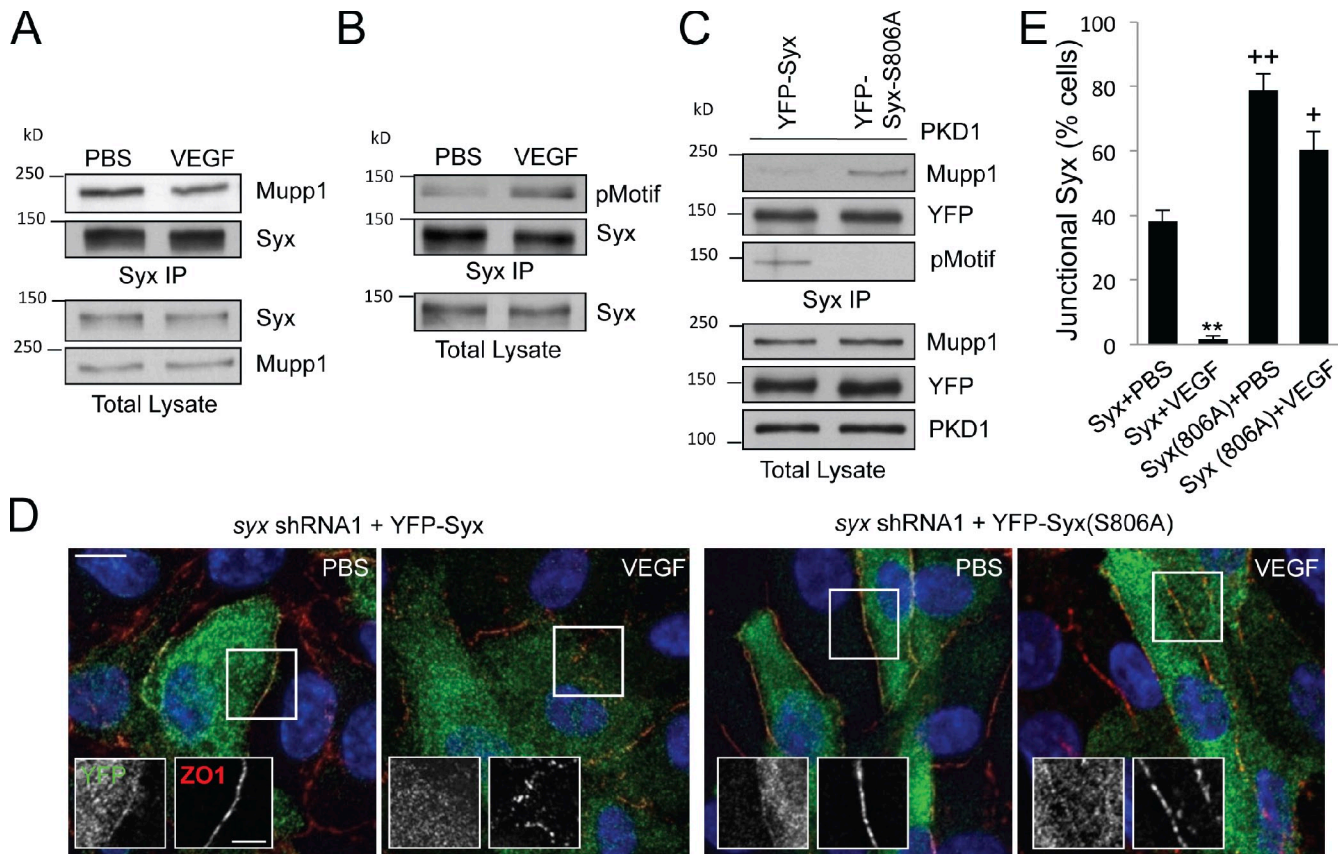
Figure 6.   **VEGF and PKD1 regulate Syx binding to Mupp1 and targeting to cell junctions.** (A) Coimmunoprecipitation of endogenous Syx with endogenous Mupp1 in HUVECs treated with either control PBS or VEGF (50 ng/ml for 30 min). (B) Detection of Syx phosphorylation at a classical PKD consensus motif by immunoblotting Syx immunoprecipitates from either PBS- or VEGF-treated cells with the pMotif antibody (pMotif). (C) Effect of the Syx S806A mutation on Mupp1 association. PKD1 was transiently coexpressed together with either YFP-Syx or YFP-Syx-S806A in HeLa cells. Syx was immunoprecipitated from cell lysates using a GFP-specific antibody, and either coprecipitated Mupp1 or PKD-mediated phosphorylation was detected using specific antibodies (Mupp1 and pMotif). (D) Effects of VEGF treatment (50 ng/ml for 30 min) on the localization of ZO1 and ectopically expressed YFP-Syx or YFP-Syx-S806A in HUVECs depleted of endogenous Syx (DAPI; blue). The framed regions of the merged image are also shown as separate YFP and ZO1 images to highlight differences in Syx and ZO1 localization. Bars: (main images) 10 µm; (insets) 5 µm. (E) Quantification of the percentage of HUVECs transfected with YFP-Syx, or YFP-Syx-S806A in fields from D, exhibiting junctional Syx staining (means ± SEM [error bars]; ∼10 cells per field; $n = 6$; +, $P < 0.01$; **/++, $P < 0.001$). IP, immunoprecipitation.

Discussion

Here, we reveal a new signaling pathway that transduces both VEGF and Ang1 signaling and explains how these ligands induce opposite effects on EC junctions and vessel permeability. The switch that determines the outcome of this pathway is the RhoA-specific GEF Syx. The removal of Syx from the junctions downstream of VEGF results in their disassembly, whereas Ang1 stabilizes junctions by activating Dia through junction-residing Syx. In addition to junction formation (Sahai and Marshall, 2002; Carramusa et al., 2007; Gavard et al., 2008), Dia reportedly also promotes focal adhesion turnover (Yamana et al., 2006). In agreement, silencing *syx* increased stress fiber density (Fig. 1 E), whereas ROCK inhibitors partially rescued junction defects induced by either Syx or Mupp1 depletion in confluent monolayers (Figs. 3 A and 4 D). These results are consistent with the antagonistic relationship between Dia and ROCK in junction maintenance (Sahai and Marshall, 2002) and suggest that Syx acts downstream of Mupp1 and the CRB complex to induce junction integrity by activating Dia and antagonizing ROCK (Fig. 7, proposed model).

The critical function of Syx in vascular homeostasis is highlighted by our observation that $syx^{-/-}$ mice exhibit EC junction defects, vascular leakiness, edema, increased passive stiffness, and lower ejection fraction. Ang1 regulates vascular leakiness, vascularization, and inflammation as well as tumor cell intra- and extravasation (Suri et al., 1996; Thurston et al., 1999, 2000; Huang et al., 2010). The observation that Syx is required for Ang1-mediated stabilization of EC junctions in vitro and in vivo is therefore consistent with the increased leakiness and the decreased vascularization of $syx^{-/-}$ mice (Garnaas et al., 2008) and raises questions as to the potential role of Syx in inflammation and/or tumor metastasis.

On the other hand, VEGF induces translocation of Syx and junction disassembly. By incorporating the new signaling events described here, PKD1 activation and phosphorylation of Syx at S^{806}, we can delineate an entire VEGF signaling pathway ending in the disassembly of cell junctions: VEGF binding to VEGFR2 (VEGF receptor 2) induces VEGFR2 autophosphorylation at Y^{1173}, which promotes the binding of PLC and subsequent activation of a PLC–IP3 pathway, leading to enhanced extracellular Ca^{2+} entry via the plasmalemmal store-operated channel

Figure 7. Schematic diagram of Syx action at endothelial junctions. (left) Syx is recruited to endothelial junctions by Mupp1 and forms a complex with multiple members of the CRB polarity complex (the asterisks denote a membrane receptor). This interaction is further promoted by Ang1 and results in the localized activation of RhoA and the selective activation of the Rho effector Dia. Dia induces junction stabilization, at least in part by suppressing the activities of Src and ROCK. (right) In contrast to Ang1, VEGF induces the dissociation of Syx from Mupp1 and its mislocalization away from cell junctions through the PKD-mediated phosphorylation of Syx at Serine 806 (pS[806]). The loss of junctional Syx/RhoA/Dia signaling results in junction disassembly, through the unopposed activities of Src and ROCK. Junction destabilization increases the permeability of confluent monolayers and induces vascular leakiness.
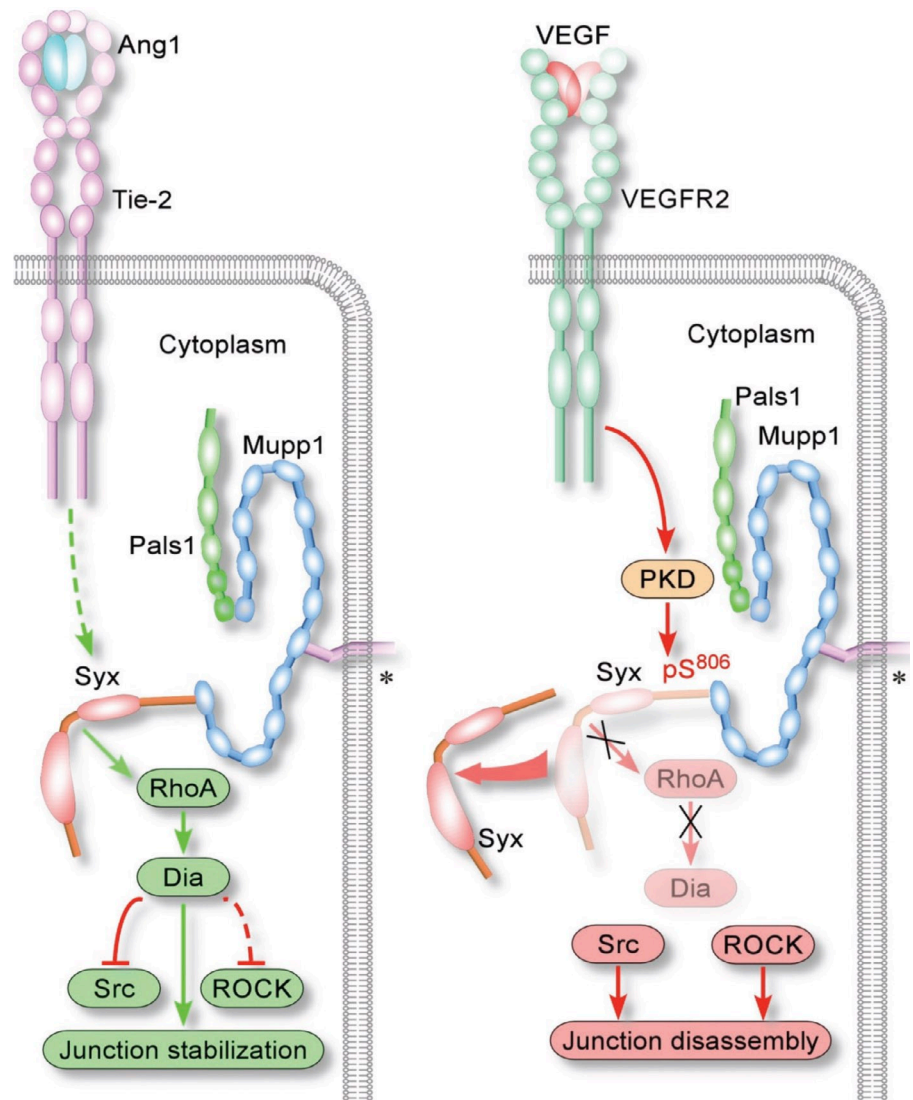
TRCP1 (transient receptor potential canonical-1; Jho et al., 2005) and the subsequent activation of PKC-α (Olsson et al., 2006). The latter then activates PKD1 by phosphorylating S^{744} and S^{748} on its activation loop (Wong and Jin, 2005). In turn, PKD1 promotes phosphorylation of Syx at S^{806}, resulting in its dissociation from Mupp1 and translocation to the cytoplasm. Removal of junctional Syx reduces Dia activity, resulting in Src activation (Gavard et al., 2008), leading to increased phosphorylation and destabilization of both AJ (Esser et al., 1998; Gavard et al., 2008) and TJ (Antonetti et al., 1999; Pedram et al., 2002) complexes, inducing junction disassembly (Fig. 7). Junction stability and barrier function are further compromised by increased contractility, presumably because of Dia deactivation and the subsequent reorganization of F-actin away from cell junctions, to focal adhesions and stress fibers (Yamana et al., 2006). Ang1 opposes VEGF-induced Ca^{2+} entry (Jho et al., 2005) and therefore PKC–PKD activation, thus providing a mechanistic explanation for its ability to retain Syx at the junctions.

PKD1 may act both upstream of RhoA by regulating Syx at the junctions and downstream of it by affecting actin dynamics. Indeed, PKD1 regulates F-actin–free barbed-end formation at the leading edge of migrating epithelial cells, downstream of RhoA and ROCK (Eiseler et al., 2009). Although this pathway has not been investigated in ECs, ROCK-activated PKD1 could further disrupt endothelial junctions by displacing Syx.

Importantly, RhoA and Src signaling have been previously implicated in several physiological and pathological conditions that depend on endothelial junction disassembly (Weis and Cheresh, 2005; Parikh et al., 2006; Gavard et al., 2008; Mackow and Gavrilovskaya, 2009). Maintaining the function of junctional Syx may therefore be therapeutically relevant in diseases characterized by vascular leakiness and edema.

Materials and methods

Cells and transfection
Heart EC isolation from adult mice (8–16 wk) followed a previously published technique (Dong et al., 1997). In brief, mouse hearts were minced and digested by collagenase I (Sigma-Aldrich). ECs were sorted by anti-Pecam1 (BD) immobilized to magnetic beads (Invitrogen), expanded, and sorted again as before, producing a >95% EC-pure preparation. The HeLa and MDCK cells were cultured in DMEM (Cellgro) with 10% fetal bovine serum (Invitrogen). HUVECs and HMVEC-dermal neonatal (Lonza) were

cultured in EGM-2 (Endothelial Growth Medium-2) and EGM-2MV, respectively (Lonza). HeLa and MDCK cells were transfected with TransIT-HeLaMONSTER (Mirus Bio LLC) and Lipofectamine 2000 (Invitrogen), respectively, according to the manufacturer's instructions. HUVEC's were transfected with HUVEC Nucleofector kit (Amaxa) according to the manufacturer's instructions.

EC-specific disruption of murine syx
LoxP sites flanking exons 10–16 (containing the catalytic Dbl homology domain of murine Syx) were inserted by homologous recombination. Heterozygous mice were crossed with germline Cre mice to excise the targeted region in all mouse tissues. Mice harboring EC-specific disruption of syx were obtained by crossing $syx^{(loxP/loxP)}$ and tie2-Cre (B6. Cg-Tg(Tek_cre)1Ywa/J; Jackson ImmunoResearch Laboratories, Inc.) mice.

Vectors, antibodies, and reagents
pEYFP-C1-mSyx, pEYFP-C1-mSyxΔPBM, N-terminally His-tagged mSyx truncation mutants, RK5-myc-LIN-7 and RK5-myc-PATJ (provided by B. Margolis, University of Michigan, Ann Arbor, MI), pEGFP-mDia1ΔN3 (provided by S. Narumiya, Kyoto University, Kyoto, Japan), and pCDNA3.1 HA-PKD wild-type, kinase-active, and kinase-dead constructs have been previously described (Kamberov et al., 2000; Ishizaki et al., 2001; Wang et al., 2004; Döppler et al., 2005; Liu and Horowitz, 2006). Point mutations of serine to alanine were introduced into pEYFP-mSyx using multisite-directed mutagenesis kit (QuikChange; Agilent Technologies). mSyx truncation mutants were generated by cloning specific coding sequences (Syx N terminus, amino acids 1–300; SyxΔNΔC, amino acids 291–800; SyxΔNter, amino acids 291–1,073) from pEYFP-mSyx into pEYFP-C1 using HindIII and BamHI as restriction sites. All constructs generated were sequenced to ensure no mutation was present.

The following antibodies were used: mouse anti-Plekhg5 (KIAA0720 clone 5A9; Abnova); mouse anti–E-cadherin, anti-EEA1, and anti-Mupp1 (BD); rabbit anti-Src (32G6), antiphospho-Src (Tyr416), and antimyc tag (Cell Signaling Technology); mouse anti-GFP 3E6, mouse anti-ZO1, monoclonal rabbit anti-GFP, and rabbit anti-ZO1 (Invitrogen); hamster and rat anti-Pecam1 (Thermo Fisher Scientific and BD, respectively); rabbit anti–PKC-µ, anti–14-3-3β, anti-Rho (26C4), anti-Pals1 (H-250), mouse anti-GIPC (C-9), goat anti–VE-cadherin (C-19; Santa Cruz Biotechnology, Inc.); mouse anti–VE-cadherin (BV6; EMD Millipore); mouse anti-FLAG, antipoly-Histidine, and rabbit antiactin (Sigma-Aldrich); and rabbit polyclonal antibody for pMOTIF was previously described (Döppler et al., 2005) as well as immunofluorescence-competent chicken anti–human Syx and rabbit anti-Mupp1 (provided by R. Javier, Baylor College of Medicine, Houston, TX; Lee et al., 2000; Liu and Horowitz, 2006). Phalloidin 594 (Invitrogen) was used to stain for actin filaments in immunofluorescence experiments. DAPI was used to stain nuclei. Alexa Fluor 488 and Alexa Fluor 594 fluorescently conjugated secondary antibodies were obtained from Invitrogen and Jackson ImmunoResearch Laboratories, Inc.

PMA (Sigma-Aldrich) and PP2 (EMD Millipore) were dissolved in DMSO to 100 and 10 µM, respectively. Human recombinant VEGF was dissolved in sterile PBS to 10 ng/ml (EMD Millipore). Recombinant human Ang1 was dissolved in sterile PBS to 50 ng/ml (R&D Systems). Y-27632 (Sigma-Aldrich) and H1152 (EMD Millipore) were dissolved in sterile water to 100 µM.

Affinity purification and mass spectrometry
YFP or YFP-tagged Syx was transfected into HeLa cells. Cell lysates were incubated with protein G beads (Invitrogen) precoated with anti-GFP (Invitrogen). Bound proteins were eluted, resolved by SDS-PAGE, and silver stained. Selected gel bands were destained, reduced, and alkylated before digestion with trypsin (Promega). Samples were analyzed using a hybrid mass spectrometer (ThermoFinnigan LTQ Orbitrap; Thermo Fisher Scientific). Mascot (Matrix Science) was used to search the Swiss-Prot database to identify isolated peptides.

shRNA and lentivirus production
Lentiviral vectors (pLKO) encoding a nontarget shRNA sequence along with human-specific shRNA target sequences for Syx and Mupp1 were purchased (Syx RNAi 1, TRCN0000130291; Syx RNAi 2, TRCN0000128190; Mupp1 RNAi 1, TRCN0000141979; and Mupp1 RNAi 2, TRCN0000145218; Thermo Fisher Scientific). 15 µg of packaging mix (ViraPower; Invitrogen) and 5 µg of the plasmid were transfected in 293FT cells (Invitrogen) using Lipofectamine 2000. 24 h later, the virus-containing media were harvested and used to infect HUVEC, HMVEC, or HeLa cells. Cells were selected with 2.5 µg/ml puromycin (Sigma-Aldrich) for 18–24 h.

Freshly infected HUVECs were harvested and replated in ECIS (electric cell-substrate impedance system) chambers for impedance measurements of monolayer barrier function.

Immunofluorescence, immunoprecipitation, and immunoblotting
Cells were plated on coverslips (type I collagen coated for HUVECs; fibronectin coated for HMVECs; BD), fixed with methanol or 3% paraformaldehyde as previously reported (Anastasiadis et al., 2000), and probed with primary antibodies followed by incubation with secondary antibodies. For HUVECs, 4×10^5 cells were resuspended in 100 µl EGM, plated on coverslips, and allowed to adhere for 5 min; for HMVECs, 2×10^5 cells were resuspended in 400 µl EGM-2MV, plated on coverslips, and allowed to adhere for 5 min. Medium was subsequently added into the wells, and the cell monolayer was maintained for 3 d before experiments were performed. VE-cadherin internalization experiments were performed according to Xiao et al. (2003). In brief, HUVECs were incubated in endothelium basal medium with anti–VE-cadherin (BV6) for 30 min at 4°C followed by antibody uptake for 30 min at 37°C in endothelium basal medium and then acid washed (10 min) to remove cell surface–bound antibody. Cells were then fixed and stained and then imaged at room temperature with a laser-scanning confocal microscope (LSM 510 META; Carl Zeiss) using Plan Neofluar 40×/1.3 NA or Plan Apochromat 63×/1.4 NA oil immersion objectives. Raw images acquired at the same intensity and exposure settings with the ZEN 2009 software (Carl Zeiss) were analyzed for junctional Syx or internalized VE-cadherin intensities using ImageJ (National Institutes of Health). Endogenous Syx was immunoprecipitated by a mouse monoclonal antibody (KIAA0720; Abnova). Protein samples were analyzed using SDS-PAGE, transferred to nitrocellulose, and probed with primary antibodies. Peroxidase-conjugated secondary antibodies (Jackson ImmunoResearch Laboratories, Inc.) were detected by luminescence (GE Healthcare).

Impedance measurement of endothelial barrier function
An electric cell substrate impedance system (ECIS Z; Applied BioPhysics) was used to measure the impedance of either HUVEC or primary mouse EC monolayers, as previously described in detail by Tiruppathi et al. (1992). In brief, cells (HUVECs, 10^5 cells/well; primary mouse ECs, 5×10^4 cells/well) were plated in ECIS Cultureware Disposable Electrode Arrays (8W10E; Applied BioPhysics) precoated with collagen. After attachment to ECIS arrays, monolayers were allowed to adhere and become quiescent for 48 h. Treatments (PBS, VEGF at 50 ng/ml, and/or Ang1 at 50 ng/ml) were added directly into the wells at the indicated times. Impedance was measured every 180 s for the duration of the entire experiment. Impedance data at 4,000 Hz, representing current flow between the cells, are presented as is or normalized to the impedance value at the beginning of the experiment. Excel (Microsoft) was used for data analysis, and Prism 4 (GraphPad Software) software was used for all graphing purposes. All data presented are representative of three independent experiments.

Rho activity assay
Rho activity was determined in HeLa cells using specific rhotekin pull-down assays (Cytoskeleton) for the activated form of the protein as previously described (Soto et al., 2008). In brief, lysates of HeLa cells transfected with the respective constructs were cleared by centrifugation and incubated with 20 µg Rhotekin–Rho-binding domain beads (Cytoskeleton) for 1 h at 4°C. Beads were then washed three times and eluted in boiling 2× Laemmli sample buffer, and the samples were analyzed by SDS-PAGE.

Electron microscopy
Mice anesthetized by 2.5% isoflurane were euthanized by injecting saturated KCl solution. Mice were perfused by PBS, pH 7.4, through the carotid artery followed by 4% paraformaldehyde, which was washed out by PBS. Hearts were fixed by 15-min immersion in 3% glutaraldehyde, 2% paraformaldehyde, and 0.1 M cacodylate buffer, pH 7.4, containing 0.1 M sucrose and 3 mM $CaCl_2$. Hearts were sliced into sections, fixed in same solution for 30 min, and cut down to ∼1-mm³ blocks followed by 24 h fixation at 4°C. Tissue blocks were fixed in 1% osmium tetroxide for 2 h and embedded in epoxy resin (Araldite; Sigma-Aldrich). Blocks were cut into 6-µm sections on a microtome. Images were acquired on a transmission electron microscope (JEM-1010; JEOL).

Microsphere extravasation
Mice anesthetized by 100 mg/kg ketamine and 10 mg/kg xylazine were injected intraperitoneally by 100 IU heparin followed by 100 µl of 1:10 diluted fluorescent 25-nm microspheres (Thermo Fisher Scientific) through

the carotid vein. The microspheres were allowed to circulate for 2 min before the chest was opened. The vascular system was perfused with 1% paraformaldehyde/PBS, pH 7.4, through the left ventricle for 2 min at a constant pressure of 120 mmHg. The trachea was removed and incubated in 1% paraformaldehyde/PBS, pH 7.4, for 2 h at room temperature and then cut longitudinally and blocked by 3% BSA in PBS with 0.3% Triton X-100 for 1 h followed by anti-Pecam1 (Thermo Fisher Scientific) and fluorescently conjugated secondary antibody. Extravasation was measured by quantifying microsphere fluorescence in each image.

Leakage of dye from skin vessels (Miles assay)
Mice anesthetized as in the previous paragraph were injected through the tail vein by 200 µl Evans blue (0.5%). After 10 min, shaved areas on the flanks of each mouse were injected by 50 µl PBS, 10 ng/ml VEGF-A$_{165}$, or 50 ng/ml Ang1. After 20 min, mice were sacrificed by cervical dislocation, and the skin around the sites of injections was dissected and flipped over to acquire digital images of dye leakage on the underside of the skin. The extent of leakage at each injection site was quantified from the images by Image-Pro (Media Cybernetics).

Pressure–volume measurements in the mouse
Mice positioned in dorsal recumbence were anesthetized with 2.5% isoflurane in oxygen, intubated, and ventilated at 133 breaths per minute with a peak inspiratory pressure <20 cm H$_2$O. Temperature was maintained at 37.5°C. Lactated Ringer's solution was delivered at 0.2 ml/h through a jugular catheter. A pressure–volume catheter (1.4 F; Millar Instruments) was inserted into the carotid artery, and the isoflurane was lowered to 1.75%. Pressure and volume were recorded with the MPVS-400 system (Millar Instruments) and analyzed by PVAN software (Millar Instruments). Baseline carotid blood pressure was recorded at the reduced isoflurane level before introducing the catheter introduced into the left ventricle. Baseline loops were recorded after a stabilization period of ~20 min. A bolus of 2–3 µl of 9% saline was injected into the jugular vein. Pressure–volume loops generated immediately after saline injection were used to determine left ventricle conductance as part of the conversion to volume units. Isoflurane levels were increased briefly to 2–2.25%, and a suture loop was placed on the transverse aorta. After a period of 10–15 min of stabilization and reduced isoflurane, the loop was tightened, and the pressure and volume were recorded immediately. This was repeated to obtain at least four series of pressure–volume loops for calculation of the end-systolic and end-diastolic pressure–volume relationship.

Statistics
Statistical significance was analyzed by Student's *t* test and expressed as a p-value.

Online supplemental material
Fig. S1 shows the interaction and colocalization of Syx with identified binding partners and the requirement of the PDZ-binding motif for these interactions. Fig. S2 shows the effects of Mupp1 and Syx depletion on junction integrity of HUVECs and HMVECs and on VE-cadherin endocytosis in HUVECs, respectively. Fig. S3 shows that the localization of Syx at areas of cell–cell contact and RhoA activation are important for cell–cell adhesion. Fig. S4 shows the VEGF/PMA-induced translocation of Syx away from junctions is caused by loss of Syx binding to Mupp1. Fig. S5 represents a series of experiments validating PKD-mediated phosphorylation of Syx at Ser[806]. Table S1 shows Syx-interacting proteins. Online supplemental material is available at http://www.jcb.org/cgi/content/full/jcb.201207009/DC1.

References

Altschmied, J., and J. Haendeler. 2008. A new kid on the block: PKD1: a promising target for antiangiogenic therapy? *Arterioscler. Thromb. Vasc. Biol.* 28:1689–1690. http://dx.doi.org/10.1161/ATVBAHA.108.174250

Anastasiadis, P.Z., S.Y. Moon, M.A. Thoreson, D.J. Mariner, H.C. Crawford, Y. Zheng, and A.B. Reynolds. 2000. Inhibition of RhoA by p120 catenin. *Nat. Cell Biol.* 2:637–644. http://dx.doi.org/10.1038/35023588

Antonetti, D.A., A.J. Barber, L.A. Hollinger, E.B. Wolpert, and T.W. Gardner. 1999. Vascular endothelial growth factor induces rapid phosphorylation of tight junction proteins occludin and zonula occluden 1. A potential mechanism for vascular permeability in diabetic retinopathy and tumors. *J. Biol. Chem.* 274:23463–23467. http://dx.doi.org/10.1074/jbc.274.33.23463

Braga, V.M., L.M. Machesky, A. Hall, and N.A. Hotchin. 1997. The small GTPases Rho and Rac are required for the establishment of cadherin-dependent cell–cell contacts. *J. Cell Biol.* 137:1421–1431. http://dx.doi.org/10.1083/jcb.137.6.1421

Carramusa, L., C. Ballestrem, Y. Zilberman, and A.D. Bershadsky. 2007. Mammalian diaphanous-related formin Dia1 controls the organization of E-cadherin-mediated cell-cell junctions. *J. Cell Sci.* 120:3870–3882. http://dx.doi.org/10.1242/jcs.014365

Cattelino, A., S. Liebner, R. Gallini, A. Zanetti, G. Balconi, A. Corsi, P. Bianco, H. Wolburg, R. Moore, B. Oreda, et al. 2003. The conditional inactivation of the β-catenin gene in endothelial cells causes a defective vascular pattern and increased vascular fragility. *J. Cell Biol.* 162:1111–1122. http://dx.doi.org/10.1083/jcb.200212157

Dejana, E., E. Tournier-Lasserve, and B.M. Weinstein. 2009. The control of vascular integrity by endothelial cell junctions: molecular basis and pathological implications. *Dev. Cell.* 16:209–221. http://dx.doi.org/10.1016/j.devcel.2009.01.004

De Toledo, M., V. Coulon, S. Schmidt, P. Fort, and A. Blangy. 2001. The gene for a new brain specific RhoA exchange factor maps to the highly unstable chromosomal region 1p36.2-1p36.3. *Oncogene.* 20:7307–7317. http://dx.doi.org/10.1038/sj.onc.1204921

Dong, Q.G., S. Bernasconi, S. Lostaglio, R.W. De Calmanovici, I. Martin-Padura, F. Breviario, C. Garlanda, S. Ramponi, A. Mantovani, and A. Vecchi. 1997. A general strategy for isolation of endothelial cells from murine tissues. Characterization of two endothelial cell lines from the murine lung and subcutaneous sponge implants. *Arterioscler. Thromb. Vasc. Biol.* 17:1599–1604. http://dx.doi.org/10.1161/01.ATV.17.8.1599

Döppler, H., P. Storz, J. Li, M.J. Comb, and A. Toker. 2005. A phosphorylation state-specific antibody recognizes Hsp27, a novel substrate of protein kinase D. *J. Biol. Chem.* 280:15013–15019. http://dx.doi.org/10.1074/jbc.C400575200

Dow, L.E., and P.O. Humbert. 2007. Polarity regulators and the control of epithelial architecture, cell migration, and tumorigenesis. *Int. Rev. Cytol.* 262:253–302. http://dx.doi.org/10.1016/S0074-7696(07)62006-3

Eiseler, T., H. Döppler, I.K. Yan, K. Kitatani, K. Mizuno, and P. Storz. 2009. Protein kinase D1 regulates cofilin-mediated F-actin reorganization and cell motility through slingshot. *Nat. Cell Biol.* 11:545–556. http://dx.doi.org/10.1038/ncb1861

Ernkvist, M., N. Luna Persson, S. Audebert, P. Lecine, I. Sinha, M. Liu, M. Schlueter, A. Horowitz, K. Aase, T. Weide, et al. 2009. The Amot/Patj/Syx signaling complex spatially controls RhoA GTPase activity in migrating endothelial cells. *Blood.* 113:244–253. http://dx.doi.org/10.1182/blood-2008-04-153874

Esser, S., M.G. Lampugnani, M. Corada, E. Dejana, and W. Risau. 1998. Vascular endothelial growth factor induces VE-cadherin tyrosine phosphorylation in endothelial cells. *J. Cell Sci.* 111:1853–1865.

Estévez, M.A., J.A. Henderson, D. Ahn, X.R. Zhu, G. Poschmann, H. Lübbert, R. Marx, and J.M. Baraban. 2008. The neuronal RhoA GEF, Tech, interacts with the synaptic multi-PDZ-domain-containing protein, MUPP1. *J. Neurochem.* 106:1287–1297. http://dx.doi.org/10.1111/j.1471-4159.2008.05472.x

Feng, Y., M.H. Chen, I.P. Moskowitz, A.M. Mendonza, L. Vidali, F. Nakamura, D.J. Kwiatkowski, and C.A. Walsh. 2006. Filamin A (FLNA) is required for cell-cell contact in vascular development and cardiac morphogenesis. *Proc. Natl. Acad. Sci. USA.* 103:19836–19841. http://dx.doi.org/10.1073/pnas.0609628104

Fischer, U.M., C.S. Cox Jr., R.H. Stewart, G.A. Laine, and S.J. Allen. 2006. Impact of acute myocardial edema on left ventricular function. *J. Invest. Surg.* 19:31–38. http://dx.doi.org/10.1080/08941930500444438

Fukata, M., M. Nakagawa, and K. Kaibuchi. 2003. Roles of Rho-family GTPases in cell polarisation and directional migration. *Curr. Opin. Cell Biol.* 15:590–597. http://dx.doi.org/10.1016/S0955-0674(03)00097-8

Garnaas, M.K., K.L. Moodie, M.L. Liu, G.V. Samant, K. Li, R. Marx, J.M. Baraban, A. Horowitz, and R. Ramchandran. 2008. Syx, a RhoA guanine exchange factor, is essential for angiogenesis in Vivo. *Circ. Res.* 103:710–716. http://dx.doi.org/10.1161/CIRCRESAHA.108.181388

Gavard, J., V. Patel, and J.S. Gutkind. 2008. Angiopoietin-1 prevents VEGF-induced endothelial permeability by sequestering Src through mDia. *Dev. Cell.* 14:25–36. http://dx.doi.org/10.1016/j.devcel.2007.10.019

Ha, C.H., and Z.G. Jin. 2009. Protein kinase D1, a new molecular player in VEGF signaling and angiogenesis. *Mol. Cells.* 28:1–5. http://dx.doi.org/10.1007/s10059-009-0109-9

Hall, A. 2005. Rho GTPases and the control of cell behaviour. *Biochem. Soc. Trans.* 33:891–895. http://dx.doi.org/10.1042/BST20050891

Huang, H., A. Bhat, G. Woodnutt, and R. Lappe. 2010. Targeting the ANGPT-TIE2 pathway in malignancy. *Nat. Rev. Cancer.* 10:575–585. http://dx.doi.org/10.1038/nrc2894

Iden, S., and J.G. Collard. 2008. Crosstalk between small GTPases and polarity proteins in cell polarization. *Nat. Rev. Mol. Cell Biol.* 9:846–859. http://dx.doi.org/10.1038/nrm2521

Ishizaki, T., Y. Morishima, M. Okamoto, T. Furuyashiki, T. Kato, and S. Narumiya. 2001. Coordination of microtubules and the actin cytoskeleton by the Rho effector mDia1. *Nat. Cell Biol.* 3:8–14. http://dx.doi.org/10.1038/35050598

Jho, D., D. Mehta, G. Ahmmed, X.P. Gao, C. Tiruppathi, M. Broman, and A.B. Malik. 2005. Angiopoietin-1 opposes VEGF-induced increase in endothelial permeability by inhibiting TRPC1-dependent Ca2 influx. *Circ. Res.* 96:1282–1290. http://dx.doi.org/10.1161/01.RES.0000171894.03801.03

Kamberov, E., O. Makarova, M. Roh, A. Liu, D. Karnak, S. Straight, and B. Margolis. 2000. Molecular cloning and characterization of Pals, proteins associated with mLin-7. *J. Biol. Chem.* 275:11425–11431. http://dx.doi.org/10.1074/jbc.275.15.11425

Katz, A.M. 2006. Physiology of the Heart. Fourth edition. Lippincott Williams & Wilkins, Philadelphia. 644 pp.

Klebes, A., and E. Knust. 2000. A conserved motif in Crumbs is required for E-cadherin localisation and zonula adherens formation in *Drosophila*. *Curr. Biol.* 10:76–85. http://dx.doi.org/10.1016/S0960-9822(99)00277-8

Lee, S.S., B. Glaunsinger, F. Mantovani, L. Banks, and R.T. Javier. 2000. Multi-PDZ domain protein MUPP1 is a cellular target for both adenovirus E4-ORF1 and high-risk papillomavirus type 18 E6 oncoproteins. *J. Virol.* 74:9680–9693. http://dx.doi.org/10.1128/JVI.74.20.9680-9693.2000

Liu, M., and A. Horowitz. 2006. A PDZ-binding motif as a critical determinant of Rho guanine exchange factor function and cell phenotype. *Mol. Biol. Cell.* 17:1880–1887. http://dx.doi.org/10.1091/mbc.E06-01-0002

Mackow, E.R., and I.N. Gavrilovskaya. 2009. Hantavirus regulation of endothelial cell functions. *Thromb. Haemost.* 102:1030–1041.

Marx, R., J. Henderson, J. Wang, and J.M. Baraban. 2005. Tech: a RhoA GEF selectively expressed in hippocampal and cortical neurons. *J. Neurochem.* 92:850–858. http://dx.doi.org/10.1111/j.1471-4159.2004.02930.x

Miyamoto, M., D.E. McClure, E.R. Schertel, P.J. Andrews, G.A. Jones, J.W. Pratt, P. Ross, and P.D. Myerowitz. 1998. Effects of hypoproteinemia-induced myocardial edema on left ventricular function. *Am. J. Physiol.* 274:H937–H944.

Olsson, A.K., A. Dimberg, J. Kreuger, and L. Claesson-Welsh. 2006. VEGF receptor signalling - in control of vascular function. *Nat. Rev. Mol. Cell Biol.* 7:359–371. http://dx.doi.org/10.1038/nrm1911

Parikh, S.M., T. Mammoto, A. Schultz, H.T. Yuan, D. Christiani, S.A. Karumanchi, and V.P. Sukhatme. 2006. Excess circulating angiopoietin-2 may contribute to pulmonary vascular leak in sepsis in humans. *PLoS Med.* 3:e46. http://dx.doi.org/10.1371/journal.pmed.0030046

Pedram, A., M. Razandi, and E.R. Levin. 2002. Deciphering vascular endothelial cell growth factor/vascular permeability factor signaling to vascular permeability. Inhibition by atrial natriuretic peptide. *J. Biol. Chem.* 277:44385–44398. http://dx.doi.org/10.1074/jbc.M202391200

Popoff, M.R., and B. Geny. 2009. Multifaceted role of Rho, Rac, Cdc42 and Ras in intercellular junctions, lessons from toxins. *Biochim. Biophys. Acta.* 1788:797–812. http://dx.doi.org/10.1016/j.bbamem.2009.01.011

Qin, Y., C. Capaldo, B.M. Gumbiner, and I.G. Macara. 2005. The mammalian Scribble polarity protein regulates epithelial cell adhesion and migration through E-cadherin. *J. Cell Biol.* 171:1061–1071. http://dx.doi.org/10.1083/jcb.200506094

Roh, M.H., O. Makarova, C.J. Liu, K. Shin, S. Lee, S. Laurinec, M. Goyal, R. Wiggins, and B. Margolis. 2002. The Maguk protein, Pals1, functions as an adapter, linking mammalian homologues of Crumbs and Discs Lost. *J. Cell Biol.* 157:161–172. http://dx.doi.org/10.1083/jcb.200109010

Sahai, E., and C.J. Marshall. 2002. ROCK and Dia have opposing effects on adherens junctions downstream of Rho. *Nat. Cell Biol.* 4:408–415. http://dx.doi.org/10.1038/ncb796

Shin, K., S. Straight, and B. Margolis. 2005. PATJ regulates tight junction formation and polarity in mammalian epithelial cells. *J. Cell Biol.* 168:705–711. http://dx.doi.org/10.1083/jcb.200408064

Soto, E., M. Yanagisawa, L.A. Marlow, J.A. Copland, E.A. Perez, and P.Z. Anastasiadis. 2008. p120 catenin induces opposing effects on tumor cell growth depending on E-cadherin expression. *J. Cell Biol.* 183:737–749. http://dx.doi.org/10.1083/jcb.200805113

Spindler, V., N. Schlegel, and J. Waschke. 2010. Role of GTPases in control of microvascular permeability. *Cardiovasc. Res.* 87:243–253. http://dx.doi.org/10.1093/cvr/cvq086

Straight, S.W., J.N. Pieczynski, E.L. Whiteman, C.J. Liu, and B. Margolis. 2006. Mammalian lin-7 stabilizes polarity protein complexes. *J. Biol. Chem.* 281:37738–37747. http://dx.doi.org/10.1074/jbc.M607059200

Suri, C., P.F. Jones, S. Patan, S. Bartunkova, P.C. Maisonpierre, S. Davis, T.N. Sato, and G.D. Yancopoulos. 1996. Requisite role of angiopoietin-1, a ligand for the TIE2 receptor, during embryonic angiogenesis. *Cell.* 87:1171–1180. http://dx.doi.org/10.1016/S0092-8674(00)81813-9

Takaishi, K., T. Sasaki, H. Kotani, H. Nishioka, and Y. Takai. 1997. Regulation of cell–cell adhesion by rac and rho small G proteins in MDCK cells. *J. Cell Biol.* 139:1047–1059. http://dx.doi.org/10.1083/jcb.139.4.1047

Taylor, C.J., K. Motamed, and B. Lilly. 2006. Protein kinase C and downstream signaling pathways in a three-dimensional model of phorbol ester-induced angiogenesis. *Angiogenesis.* 9:39–51. http://dx.doi.org/10.1007/s10456-006-9028-y

Tepass, U. 1996. Crumbs, a component of the apical membrane, is required for zonula adherens formation in primary epithelia of *Drosophila. Dev. Biol.* 177:217–225. http://dx.doi.org/10.1006/dbio.1996.0157

Terry, S.J., C. Zihni, A. Elbediwy, E. Vitiello, I.V. Leefa Chong San, M.S. Balda, and K. Matter. 2011. Spatially restricted activation of RhoA signalling at epithelial junctions by p114RhoGEF drives junction formation and morphogenesis. *Nat. Cell Biol.* 13:159–166. http://dx.doi.org/10.1038/ncb2156

Thurston, G., C. Suri, K. Smith, J. McClain, T.N. Sato, G.D. Yancopoulos, and D.M. McDonald. 1999. Leakage-resistant blood vessels in mice transgenically overexpressing angiopoietin-1. *Science.* 286:2511–2514. http://dx.doi.org/10.1126/science.286.5449.2511

Thurston, G., J.S. Rudge, E. Ioffe, H. Zhou, L. Ross, S.D. Croll, N. Glazer, J. Holash, D.M. McDonald, and G.D. Yancopoulos. 2000. Angiopoietin-1 protects the adult vasculature against plasma leakage. *Nat. Med.* 6:460–463. http://dx.doi.org/10.1038/74725

Tiruppathi, C., A.B. Malik, P.J. Del Vecchio, C.R. Keese, and I. Giaever. 1992. Electrical method for detection of endothelial cell shape change in real time: assessment of endothelial barrier function. *Proc. Natl. Acad. Sci. USA.* 89:7919–7923. http://dx.doi.org/10.1073/pnas.89.17.7919

Wang, Q., T.W. Hurd, and B. Margolis. 2004. Tight junction protein Par6 interacts with an evolutionarily conserved region in the amino terminus of PALS1/stardust. *J. Biol. Chem.* 279:30715–30721. http://dx.doi.org/10.1074/jbc.M401930200

Watanabe, N., T. Kato, A. Fujita, T. Ishizaki, and S. Narumiya. 1999. Cooperation between mDia1 and ROCK in Rho-induced actin reorganization. *Nat. Cell Biol.* 1:136–143. http://dx.doi.org/10.1038/11056

Weis, S.M., and D.A. Cheresh. 2005. Pathophysiological consequences of VEGF-induced vascular permeability. *Nature.* 437:497–504. http://dx.doi.org/10.1038/nature03987

Wojciak-Stothard, B., and A.J. Ridley. 2002. Rho GTPases and the regulation of endothelial permeability. *Vascul. Pharmacol.* 39:187–199. http://dx.doi.org/10.1016/S1537-1891(03)00008-9

Wong, C., and Z.G. Jin. 2005. Protein kinase C-dependent protein kinase D activation modulates ERK signal pathway and endothelial cell proliferation by vascular endothelial growth factor. *J. Biol. Chem.* 280:33262–33269. http://dx.doi.org/10.1074/jbc.M503198200

Xiao, K., D.F. Allison, K.M. Buckley, M.D. Kottke, P.A. Vincent, V. Faundez, and A.P. Kowalczyk. 2003. Cellular levels of p120 catenin function as a set point for cadherin expression levels in microvascular endothelial cells. *J. Cell Biol.* 163:535–545. http://dx.doi.org/10.1083/jcb.200306001

Yamana, N., Y. Arakawa, T. Nishino, K. Kurokawa, M. Tanji, R.E. Itoh, J. Monypenny, T. Ishizaki, H. Bito, K. Nozaki, et al. 2006. The Rho-mDia1 pathway regulates cell polarity and focal adhesion turnover in migrating cells through mobilizing Apc and c-Src. *Mol. Cell. Biol.* 26:6844–6858. http://dx.doi.org/10.1128/MCB.00283-06